

## Direct observation of Si lattice strain and its distribution in the Si(001)–SiO<sub>2</sub> interface transition layer

Young Pil Kim, Si Kyung Choi, Hyun Kyong Kim, and Dae Won Moon

Citation: *Appl. Phys. Lett.* **71**, 3504 (1997); doi: 10.1063/1.120373

View online: <http://dx.doi.org/10.1063/1.120373>

View Table of Contents: <http://apl.aip.org/resource/1/APPLAB/v71/i24>

Published by the [American Institute of Physics](#).

---

### Additional information on *Appl. Phys. Lett.*

Journal Homepage: <http://apl.aip.org/>

Journal Information: [http://apl.aip.org/about/about\\_the\\_journal](http://apl.aip.org/about/about_the_journal)

Top downloads: [http://apl.aip.org/features/most\\_downloaded](http://apl.aip.org/features/most_downloaded)

Information for Authors: <http://apl.aip.org/authors>

## ADVERTISEMENT



**Goodfellow**  
metals • ceramics • polymers • composites  
70,000 products  
450 different materials  
**small quantities fast**

[www.goodfellowusa.com](http://www.goodfellowusa.com)

# Direct observation of Si lattice strain and its distribution in the Si(001)–SiO<sub>2</sub> interface transition layer

Young Pil Kim<sup>a)</sup> and Si Kyung Choi

Department of Materials Science and Engineering, Korea Advanced Institute of Science and Technology, Taejon 305-701, Korea

Hyun Kyong Kim and Dae Won Moon<sup>b)</sup>

Surface Analysis Group, Korea Research Institute of Standards and Science, Taejon 305-606, Korea

(Received 4 August 1997; accepted for publication 11 October 1997)

In the transition layer of the Si(001)–SiO<sub>2</sub> interface, Si lattice strain and its distribution were directly observed by medium energy ion scattering spectroscopy for thermal and ion beam oxides. The strain was in the vertical direction, and the maximum values at the SiO<sub>2</sub> side of the transition layer were 0.96% and 2.8% for the thermal and ion beam oxides, respectively. © 1997 American Institute of Physics. [S0003-6951(97)00750-X]

The Si(001)–SiO<sub>2</sub> interface has been intensively investigated with various experimental techniques due to its importance in improving the electronic properties of ultrathin SiO<sub>2</sub> dielectric layers and silicon-on-insulators. Previous experiments<sup>1–8</sup> have reported 0.5–25 nm thick transition layers at the interface, presenting different aspects of the compositional and structural transition depending on the analysis methods used. However, detailed information on the transition layer is still not sufficient for a clear understanding of how the interface is formed between a crystalline Si substrate and an amorphous SiO<sub>2</sub> overlayer.

We report here a direct observation of strained Si lattices and their strain distribution in the transition layers of the Si(001)–SiO<sub>2</sub> interfaces with medium energy ion scattering (MEIS) spectroscopy for thermal and ion beam oxides formed by O<sub>2</sub><sup>+</sup> ion beam bombardment. Compared with other structural analysis methods based on diffraction, MEIS measurements can provide simple and direct structural information in real space with depth resolution of a couple of atomic layers, from the blocking dip position and the electronic energy loss analysis.<sup>9</sup> We believe the information in this letter is useful in order to understand more clearly the still controversial structure of the Si(001)–SiO<sub>2</sub> interface.

The Si(001)–SiO<sub>2</sub> interfaces formed by thermal oxidation and O<sub>2</sub><sup>+</sup> ion beam oxidation were investigated. Two kinds of thermal oxides were analyzed. One was a 5.5 nm thermal oxide, grown by a semiconductor company according to its gate oxide growing process; the other was a 3 nm thermal oxide grown in a reactor chamber connected to our MEIS system by heating a Si(001) wafer to 780 °C in an atmospheric oxygen and nitrogen mixture. The ion beam oxides were made in the MEIS chamber by 3 keV O<sub>2</sub><sup>+</sup> ion bombardment in the surface normal direction up to the ion dose of  $5 \times 10^{17}$  atoms cm<sup>-2</sup>. After ion beam oxidation, the samples were annealed at 1200 °C for 15 s in 99% Ar + 1% O<sub>2</sub> ambient. The ion beam oxides before and after annealing were analyzed by MEIS.

In the MEIS analysis, a 97.8 keV proton beam was aligned along the [11 $\bar{1}$ ] direction, and the protons scattered from Si atoms along the [001] direction were analyzed in the double alignment condition with scattering angle 125.3°. The energy spectra are given in Fig. 1. Blocking dips around the [111] direction in Fig. 2 were measured in the single alignment condition, with the incident ion beams at 2.5° from the [00 $\bar{1}$ ] direction, to improve counting statistics. The angular resolution, determined mainly by the incident ion beam divergence and the position sensitive detector, was estimated to be about 0.1°. During MEIS experiments, the damage to the specimen by the proton beam was kept below a 5% Si surface peak area increase. Details of MEIS and our system have been described elsewhere.<sup>9,10</sup>

The energy spectra in Fig. 1 were fitted by simulations that calculate the energy and intensities of the backscattered particles scattered from thin slabs in the specimen. The program written by Kido *et al.*<sup>11</sup> was modified to treat the crystallinity of each layer. In the simulation, we treated the interface layer as consisting of several layers of which the

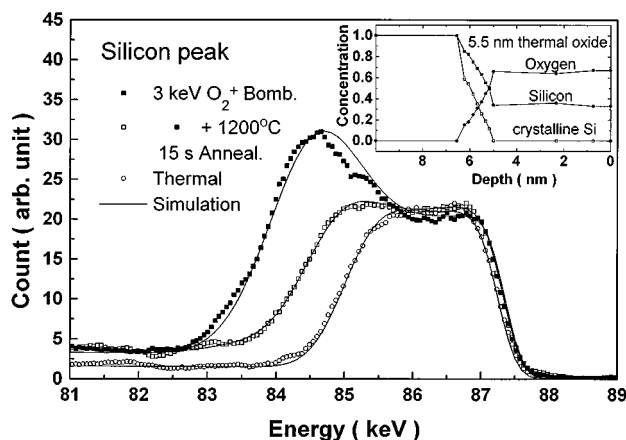


FIG. 1. The Si peaks in the energy spectra for a 5.5 nm thick thermal oxide and an ion beam oxide made by 3 keV O<sub>2</sub><sup>+</sup> ion bombardment before and after annealing. 97.8 keV H<sup>+</sup> ions were incident in the [11 $\bar{1}$ ] direction and the protons scattered in the [001] direction were measured. The Si and O concentration profiles and the Si crystallinity profile used in the simulation are given in the inset and the simulated energy spectra are shown with the measured energy spectra.

<sup>a)</sup>Present address: Semiconductor R&D Center, Samsung Electronics, Co. Ltd., Kyungki-do 449-900, Korea.

Electronic mail: ypilkim@samsung.co.kr

<sup>b)</sup>Corresponding author. Electronic mail: dwmoon@krissol.krissl.re.kr

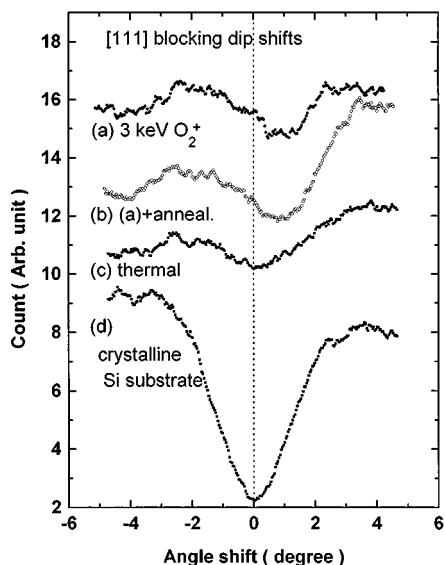


FIG. 2. The blocking dips of Si peaks in the transition layers of a thermal oxide and ion beam oxides before and after annealing, in the [111] directions. These blocking dips were measured with the incident  $H^+$  beam at  $2.5^\circ$  from the [001] direction.

composition changed gradually from amorphous  $SiO_2$  to crystalline Si. The absence of a hump in the Si peak of the transition layer for the thermal oxide in Fig. 1 indicates that the transition layer is not completely amorphous. Therefore a crystallinity factor, which represents the ratio of the crystalline Si atoms to the total Si atoms in each layer, was used in the simulations. This factor was used to calculate the energy loss, dechanneling fraction and Si peak intensity. The effect of the roughness was not considered in the simulation.

From the simulation result in the inset of Fig. 1 for the thermal oxide, the numbers of Si and O atoms in the interface layer were  $(4.7 \pm 0.5) \times 10^{15} \text{ cm}^{-2}$  and  $(2.5 \pm 0.3) \times 10^{15} \text{ cm}^{-2}$ , respectively. The number of ordered crystalline Si atoms was  $(2.3 \pm 0.5) \times 10^{15} \text{ cm}^{-2}$ , which is about half of the total Si atoms in the transition layer. Consequently, the number of remaining Si atoms is  $(2.4 \pm 0.5) \times 10^{15} \text{ cm}^{-2}$ , which could be in the form of either  $SiO_2$  or Si suboxide. The fraction of Si atoms in the intermediate oxidation states depends on the local distribution of oxygen in the transition layer and the morphology of the interface. If we assume that all the  $2.5 \times 10^{15} \text{ cm}^{-2}$  oxygen atoms are used to form  $SiO_2$ , consuming  $1.25 \times 10^{15} \text{ cm}^{-2}$  Si atoms, then the remaining  $(1.2 \pm 0.5) \times 10^{15} \text{ cm}^{-2}$  Si atoms can be considered as Si atoms in an intermediate oxidation state located at the boundary between the  $SiO_2$  and the crystalline Si. The density of Si atoms in intermediate oxidation states in the transition layer,  $(1.5 \pm 0.5) \times 10^{15} \text{ cm}^{-2}$  as reported by Himpfel *et al.*,<sup>3</sup> is close to the minimum limit  $(1.2 \pm 0.5) \times 10^{15} \text{ cm}^{-2}$  estimated above, which suggests that the majority of the oxygen atoms in the transition layer are used to form  $SiO_2$ . The thickness of the interface with  $(4.7 \pm 0.5) \times 10^{15} \text{ Si atoms cm}^{-2}$  corresponds to  $(1.3 \pm 0.2) \text{ nm}$  considering the volume expansion due to Si oxidation, which is very similar to the value reported by a previous MEIS analysis.<sup>7</sup> The results for 3 nm thermal oxide grown in the reactor chamber were very similar to the above.

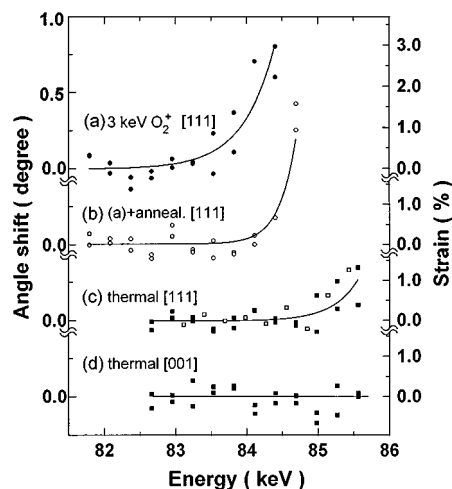


FIG. 3. The shift of the blocking dip positions of Si peaks for ion beam oxides before (a) and after (b) annealing and a 5.5 nm thermal oxide (c), in the [111] direction. The dip positions in the [001] direction are given in (d). Open square points in (c) are for a 3 nm thermal oxide. They were shifted by 1 keV due to the different oxide thickness, to be compared on the same energy scale.

The areal density of Si in the transition layer of the ion beam oxides before annealing were about four times larger than that of the thermal oxides, mainly due to the presence of the  $3.7 \times 10^{15} \text{ cm}^{-2}$  amorphous Si layer. After annealing, the areal density decreased as the amorphous Si in the transition layer recrystallized, as shown in Fig. 1. But the interface was still much broader than for the thermal oxide with higher Si/O ratio.

The presence of Si crystallines and their distribution in the transition layer can be seen clearly in the blocking dips of the Si peak given in Fig. 2 for the thermal oxides and ion beam oxides. The deep blocking dips in the bulk Si change to shallow dips in the transition layer, which means that the crystallinity in the transition layer is smaller than in the substrate crystalline Si. The blocking dips shown in Fig. 2 were taken at the  $SiO_2$  side of the interfaces. Simulations are in progress to fit the blocking dip shapes, which may provide more detailed information on the Si crystalline lattices at the transition layer.

The most interesting and important observation in this letter is the shift of the [111] blocking dips in the interface layer to higher scattering angles with respect to the dips in the bulk Si, as shown in Fig. 2. The changes of the dip positions as a function of the depth from the interface are plotted in Fig. 3. However, the [001] blocking dip position at the transition layer did not shift from the dip position of the bulk Si, as shown in Fig. 3(d) for thermal oxides. The ion beam oxides did not show any shift in the [001] blocking dip position either before or after annealing. The blocking dip shifts for the thermal oxides were smaller than those for the ion beam oxides. To confirm the dip position shift for the thermal oxides, another 3 nm thermal oxide made *in situ* was analyzed with similar results, drawn in open squares in Fig. 3(c).

From Fig. 3, it is clear that there are shifts in the [111] dip positions for the thermal oxides and the ion beam oxides before and after annealing, but no shifts for the [001] dips.

The maximum shifts of the [111] dip positions were  $(0.26 \pm 0.14)^\circ$  and  $(0.77 \pm 0.13)^\circ$  for the thermal oxide and the ion beam oxide, respectively. Annealing of the SiO<sub>2</sub> layer made by oxygen ion beam bombardment did not change the maximum shift in the dip position, even though the transition layer thickness decreased significantly. Based on a simple trigonometric estimation, the above angular shifts of [111] dips can be converted to 0.0011 nm and 0.0038 nm vertical displacements of the Si atoms, which correspond to 0.96% and 2.8% strains calculated from  $\Delta d_{[001]}/d_{[001]}$ , where  $d_{[001]}$  is the (001) interlayer distance, 0.136 nm.<sup>9</sup>

The strain in the vertical direction of the Si lattices in the interface could be understood in terms of stress due to the volume expansion from Si oxidation. During the oxidation, oxidized Si can expand freely in the vertical direction but not in the lateral direction. The lateral expansion compresses the neighboring Si lattices within the transition layer, and the Si lattices will expand in the vertical direction. In concert with this, the vertical expansion of oxidized Si would pull up the neighboring Si lattices in the surface normal direction. However, lateral displacement was not observed in this experiment. Another possibility is the Si lattice expansion due to Si interstitials diffused from the oxide layer. It has been reported that excess Si atoms are emitted into interstitial sites during Si oxidation to reduce the stress-strain energy.<sup>12–15</sup> These effects could be enhanced by the forced O<sub>2</sub><sup>+</sup> ion incorporation and the extra Si interstitials due to direct recoil or ion beam mixing for ion beam oxides. Consequently, the displacement of the Si in the transition layer for ion beam oxides can be much larger than that of thermal oxides.

In summary, the compositional and structural changes in the transition layer of the Si(001)–SiO<sub>2</sub> interfaces for ther-

mal oxides and ion beam oxides were measured by MEIS. The presence of crystalline Si lattices in the transition layer was clearly observed in the energy spectra and the blocking dips. From the shift of the blocking dip position, the strain of the crystalline Si lattices and its distribution in the transition layer could be measured. The strains were in the vertical direction and the maximum values were 0.96% and 2.8% for the thermal oxides and the ion beam oxides, respectively.

Financial support from the Center for Molecular Science, Korea, and the Ministry of Science and Technology, Korea, is appreciated. The authors thank Y. Kido and K. Koshikawa for providing the program to calculate the energy spectra.

<sup>1</sup>A. Ourmazd, D. W. Taylor, J. A. Rentschler, and J. Bevk, *Phys. Rev. Lett.* **59**, 213 (1987).

<sup>2</sup>H. Akatsu, Y. Sumi, and I. Ohdomari, *Phys. Rev. B* **44**, 1616 (1991).

<sup>3</sup>F. J. Himpsel, F. R. McFeely, A. Taleb-Ibrahimi, J. A. Yarmoff, and G. Hollinger, *Phys. Rev. B* **38**, 6084 (1988).

<sup>4</sup>K. Ohishi and T. Hattori, *Jpn. J. Appl. Phys., Part 2* **33**, L675 (1994).

<sup>5</sup>L. C. Feldman, P. J. Silverman, J. S. Williams, T. E. Jackman, and I. Stensgaard, *Phys. Rev. Lett.* **41**, 1396 (1978).

<sup>6</sup>R. Haight and L. C. Feldman, *J. Appl. Phys.* **53**, 4884 (1982).

<sup>7</sup>E. P. Gusev, H. C. Lu, T. Gustafsson, and E. Garfunkel, *Phys. Rev. B* **52**, 1759 (1995).

<sup>8</sup>P. H. Fuoss, L. J. Norton, S. Brennan, and A. Fischer-Colbrie, *Phys. Rev. Lett.* **60**, 600 (1988).

<sup>9</sup>J. F. van der Veen, *Surf. Sci. Rep.* **5**, 199 (1985).

<sup>10</sup>J. C. Lee, C. S. Chung, H. J. Kang, Y. P. Kim, H. K. Kim, and D. W. Moon, *J. Vac. Sci. Technol. A* **13**, 1325 (1995).

<sup>11</sup>Y. Kido and T. Koshikawa, *J. Appl. Phys.* **67**, 187 (1990).

<sup>12</sup>G. Lüpke, D. J. Bottomley, and H. M. van Driel, *Phys. Rev. B* **47**, 10389 (1993).

<sup>13</sup>G. Renaud, P. H. Fuoss, A. Ourmazd, J. Bevk, B. S. Freer, and P. O. Hahn, *Appl. Phys. Lett.* **58**, 1044 (1991).

<sup>14</sup>A. Stesmans, *Phys. Rev. B* **48**, 2418 (1993).

<sup>15</sup>B. Leroy, *Philos. Mag. B* **55**, 159 (1987).